CONFERENCE PRE-PRINT

WALL CONDITIONING PLASMA PRODUCTION USING FUNDAMENTAL AND SECOND HARMONIC ELECTRON CYCLOTRON WAVES IN JT-60SA

M. FUKUMOTO, T. WAKATSUKI, S. KOJIMA, T. NAKANO National Institutes for Quantum Science and Technology, Naka/Ibaraki, Japan

Email: fukumoto.masakatsu@qst.go.jp

Abstract

Four sequences of Electron Cyclotron Wall Conditioning with He working gas (He-ECWC) were conducted following H₂ tokamak discharges, resulting in the removal of 16% of the H₂ molecules retained by the previous H₂ tokamak discharges. The He-ECWC plasma produced by a fundamental ordinary mode (O1-mode) EC wave at a frequency of f_{EC} = 82 GHz expanded along the poloidal magnetic field lines. The highest H₂ removal ratio relative to the residual H₂ molecules was obtained under the poloidal magnetic field in a Trapped Particle Configuration (TPC) with an *n*-index of 0.7 at toroidal magnetic fields of B_T = 1.79 and 2.04 T. A comparable H₂ removal ratio was observed in a horizontal magnetic configuration at B_T = 1.79 T. In contrast, He-ECWC plasma produced by a second harmonic extraordinary mode (X2-mode) EC wave at f_{EC} = 110 GHz was localized and did not show significant variation in H₂ removal across different poloidal magnetic configurations in the TPC at B_T = 1.79 and 2.04 T. No He-ECWC plasma was observed in the horizontal magnetic configuration at B_T = 1.79 and 2.04 T. The temperature increase of the carbon tiles facing to the EC launcher during the one pulse of the He-ECWC was consistent with that observed during EC wave irradiation without plasma within the variation (\pm 20%), indicating that the first-pass absorption rates of the O1-mode and X2-mode EC wave.

1. INTRODUCTION

Inter-shot wall conditioning is an essential tool to control hydrogen recycling in tokamak devices. In tokamak devices with conducting coils, Glow Discharge Cleaning (GDC) and Taylor Discharge Cleaning (TDC) are commonly employed as an inter-shot wall conditioning tool. However, superconducting devices like JT-60SA, GDC are difficult to apply as inter-shot wall conditioning tools due to the inability to generate direct current glow discharge in the presence of a toroidal magnetic field. Similarly, TDC is hard to implement because the electric field that can be applied by Central Solenoid (CS) is limited. Alternatively, Wall Conditioning using Electron Cyclotron (ECWC) and Ion Cyclotron (ICWC) are candidates as inter-shot conditioning tools. Since JT-60SA does not equipe an IC heating system, ECWC is the only tool for the inter-shot wall conditioning.

In JT-60SA, tokamak plasma is initiated using the inboard first wall as a limiter. Therefore, removal of retained H_2 from the inboard first wall is crucial to suppress H_2 desorption during the start-

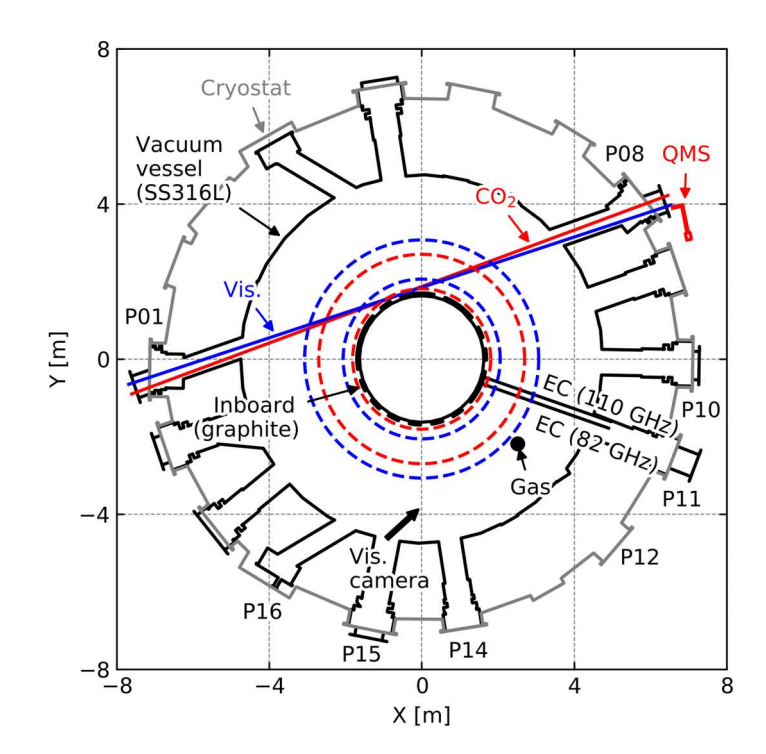


FIG. 1. Schematic view of the toroidal cross-section of JT-60SA with the diagnostics used in this study. The red broken lines at R=1.81 and 2.70 m show the fundamental and second harmonic resonance layers at $B_T=1.79$ T with $f_{EC}=82$ and 110 GHz, respectively. The blue broken lines at R=2.06 and 3.07 m show the fundamental and second harmonic resonance layers at $B_T=2.04$ T with $f_{EC}=82$ and 110 GHz, respectively.

up phase. Because EC plasma is generated at the resonance layer by resonant absorption of EC wave, the plasma produced at the resonance layer must be expanded toward the inboard first wall.

To apply He-ECWC on JT-60SA, expansion of He-ECWC plasma by poloidal magnetic configuration have been investigated in JT-60U [1]. He-ECWC plasma produced by a fundamental extraordinary mode (X1-mode) EC wave was expanded throughout the entire torus. On the other hand, expansion of He-ECWC plasma produced by a second harmonic extraordinary mode (X2-mode) EC wave was limited. These differences are attributed to variations in the absorption rates of the EC waves.

In JT-60SA, expansions of He-ECWC plasma using the O1-mode and X2-mode EC wave under the different poloidal magnetic configuration have been investigated, and influences on the amount of removed H₂ was observed. Furthermore, possible processes of plasma production by injection of the O1-mode and X2-mode EC wave were discussed based on the single-pass absorption rate of EC wave evaluated experimentally and numerically.

2. EXPERIMENTAL SETUP

Figure 1 shows a schematic view of the toroidal crosssections of JT-60SA with the diagnostics used in this study. JT-60SA has a major radius of R = 2.97 m and a minor radius of a = 1.18 m. The vacuum vessel is made of stainless steel SS316L. A part of the inboard first wall (about 61%) and the upper part of the vacuum vessel called as an upper divertor are covered by graphite tiles. The volume of the vacuum vessel is 369 m³. The pumping speed for H₂ gas is 10.8 ± 0.2 m³/s. Helium gas is injected from the bottom part of the vacuum vessel. Two electron cyclotron (EC) waves are injected from the upper oblique port in a direction normal ti the toroidal magnetic field: an ordinary mode (O-mode) EC wave with a frequency of $f_{EC} = 82$ GHz, and an extraordinary mode (X-mode) EC wave with a frequency of $f_{EC} = 110$ GHz. The wall temperature is set at 50 °C.

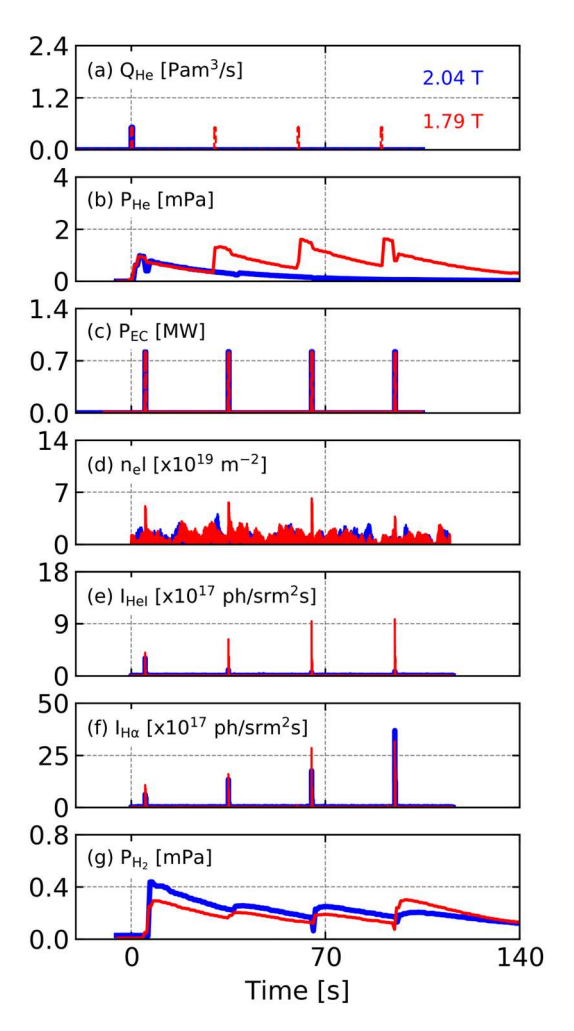


FIG. 2. Time traces of O1-mode He-ECWC sequences at $f_{EC} = 82$ GHz for $B_T = 1.79$ T (Shot No. of E101167) and 2.04 T (E101164): (a) He gas injection rate, Q_{He} , (b) He partial pressure, P_{He} , evaluated by the QMS, (c) EC injection power, P_{EC} , (d) line-integrated electron density, n_{el} , evaluated by the CO2 interferometer, (e) He I intensity, I_{Hel} , and (f) H_{α} intensity, $I_{H\alpha}$, evaluated by the visible spectrometer and (g) H2 partial pressure, P_{H2} , evaluated by the QMS. The red curves show time traces at $B_T = 1.79$ T, and the blue ones at $B_T = 2.04$ T. It is noted that He gas is injected only before the first EC pulse at $B_T = 2.04$ T.

The line-integrated electron density, n_e l, is measured using a CO₂ laser interferometer. Intensities of He I and H α emission lines are measured by a visible spectrometer. Plasma shapes are captured using a visible camera with a horizontal field of view. Partial pressures of H₂ and He gases are evaluated by a Quadrupole Mass Spectrometer (QMS) calibrated with pure gases.

3. RESULTS AND DISCUSSION

3.1. Effects of poloidal magnetic configuration on expansion of plasma produced by 82 GHz fundamental ordinary mode EC wave

Figure 2 shows time traces of O1-mode He-ECWC sequences at $f_{\rm EC}$ = 82 GHz for $B_{\rm T}$ = 1.79 and 2.04 T. After He gas was injected (Fig. 2(a)) and $P_{\rm He}$ stabilized (Fig. 2(b)), the O1-mode EC wave with $f_{\rm EC}$ = 82 GHz and $P_{\rm EC}$ = 0.8 MW was injected in the direction normal to the toroidal magnetic field with a pulse length of 0.3 s and a duty

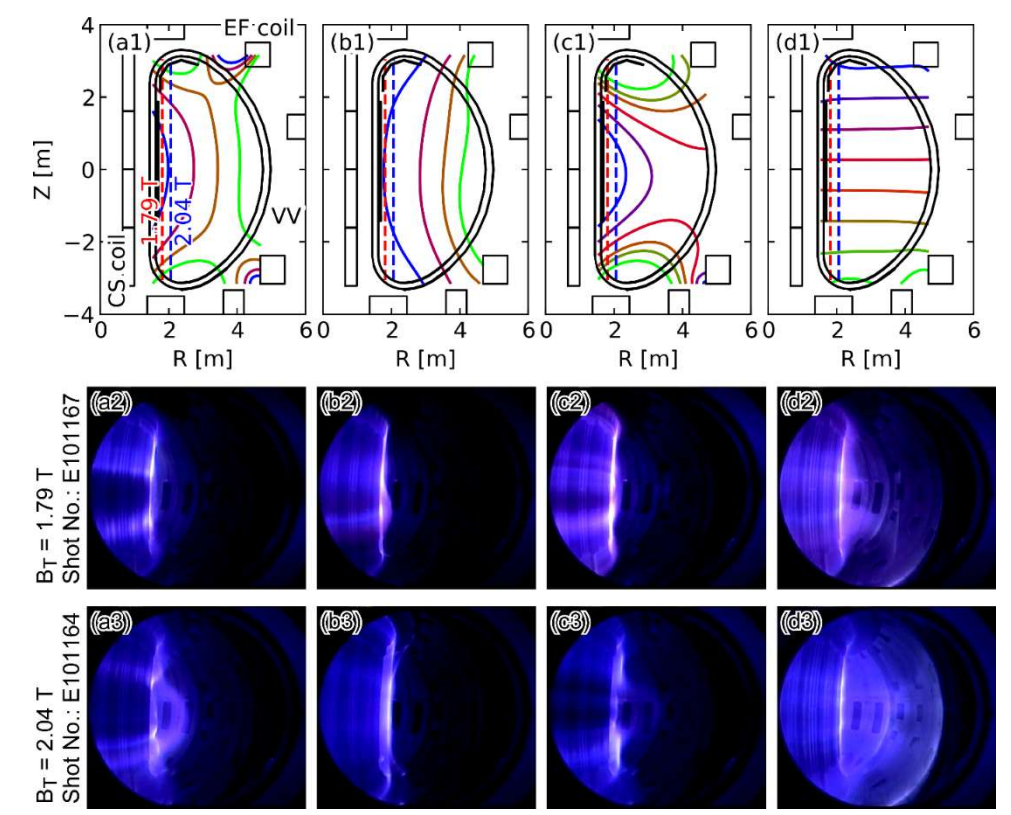


FIG. 3. Poloidal magnetic configurations for O1-mode He-ECWC experiments at $f_{EC} = 82$ GHz for $B_T = 1.79$ T and 2.04 T across four pulses, and produced He-ECWC plasmas captured by the visible camera. The poloidal magnetic configurations for (a) the first pulse with TPC with an n-index of n = 0.7, (b) the second pulse with TPC with n < 0, (c) the third pulse with TPC with n = 3 and (d) the fourth pulse with a horizontal magnetic configuration. The colored solid lines indicate the contours of magnetic flux. The red broken lines show the fundamental resonance layer at $B_T = 1.79$ T, and the blue ones at $B_T = 2.04$ T. The produced He-ECWC plasmas are captured by the visible camera at (a2–d2) $B_T = 1.79$ T and (a3–d3) 2.04 T.

cycle of 1/100 (Fig. 2(c)) under 4 different poloidal magnetic configurations as shown in Fig. 3(a1-d1). The first three pulses were conducted under a Trapped Particle Configuration (TPC) with a different n-index, while the last pulse was conducted with a horizontal magnetic configuration. The fundamental resonance layer was located at R = 1.81 m for B_T = 1.79 T and at R = 2.06 m for B_T = 2.04 T, as shown in Fig. 2. The time intervals between pulses were set to approximately 30 s because the time constant for pumping down of H_2 gas, calculated by dividing the vacuum vessel volume (369 m³) by the pumping speed for H_2 gas (10.8 m³/s), was 34 s. This time interval reduced the re-ionization and re-implantation of H_2 molecules released from the wall because the characteristic ionization time of H_2 molecules in ECWC plasma was shorter than the time constant of pumping down (a few tens of seconds). After the O1-mode EC wave with f_{EC} = 82 GHz was injected (Fig. 2(c)), n_e l and I_{HeI} increased as shown in Fig. 2(d) and (e), respectively. The intensity of the H_α signal, $I_{H\alpha}$, and P_{H2} increased, as shown in Fig. 2(f) and (g), respectively, indicating that H_2 molecules were desorbed from the wall.

Figs. 3(a2–d2) show the He-ECWC plasma produced by the O1- mode EC wave at $f_{\rm EC}$ = 82 GHz and $B_{\rm T}$ = 1.79 T, and Figs. 3(a3–d3) show that at $B_{\rm T}$ = 2.04 T. In the case of the He-ECWC under the TPC (Figs. 3(a2–c2) and 3(a3–c3)), the O1-mode He-ECWC plasma expanded along the poloidal magnetic field lines, and strong light emission was observed on the inboard first wall. For the horizontal magnetic configuration (Figs. 3(d2) and 3(d3)), the He-ECWC plasma expanded throughout the entire volume in the torus, and strong light emission was observed on the inboard first wall.

3.2. Effects of poloidal magnetic configuration on expansion of plasma produced by 110 GHz second harmonic extraordinary mode EC wave

Fig. 4 shows time traces of X2-mode He-ECWC sequences at $f_{\rm EC}$ = 110 GHz for $B_{\rm T}$ = 1.79 and 2.04 T. The experiment was performed using a procedure similar to that of the O1-mode He-ECWC. The differences from the O1-mode He-ECWC were $Q_{\rm He}$ (Fig. 4(a)), $P_{\rm He}$ (Fig. 4(b)), $P_{\rm EC}$ = 0.5 MW (Fig. 4(c)) and the poloidal magnetic

configuration at the second pulse shown in Fig. 5(b1). The second harmonic resonance layer was located at R = 2.70 m for $B_T = 1.79$ T and at R = 3.07 m for $B_T = 2.04$ T, as shown in Fig. 1.

On the X2-mode He-ECWC with $f_{\rm EC}=110$ GHz, no clear increase in $n_{\rm e}l$ was observed for either of the two $B_{\rm T}$ cases as shown in Fig. 4(d). On the other hand, $I_{\rm HeI}$ increased following the EC injection as shown in Fig. 4(e), indicating that the He-ECWC plasma was produced. The intensity of H_{α} signal, $I_{\rm H\alpha}$, and $P_{\rm H2}$ increased after the EC wave was injected as shown in Fig. 4(f) and (g), respectively, indicating that H_2 molecules were desorbed from the wall.

Figs. 5(a2–d2) show the He-ECWC plasma produced by the 110 GHz X2-mode EC wave at $B_T = 1.79$ T, and Figs. 5(a3–d3) show that at $B_T = 2.04$ T. In the case of the He-ECWC with the TPC (Figs. 5(a2-c2) and 5(a3c3)), the X2-mode He-ECWC plasma was produced locally, and the plasma did not expand along the poloidal magnetic field lines. For the horizontal magnetic configuration (Figs. 5(d2) and 5(d3)), no clear He-ECWC plasma was observed. The lack of a clear increase in $P_{\rm H2}$ at the last pulse, as shown in Fig. 4(e), was due to the insufficient plasma production. It was noted that no clear increase in $n_{\rm e}$ l shown in Fig. 4(d) was due to the local plasma production: the ECWC plasma was produced around the second harmonic resonance layer, which was outside the laser path of the CO₂ interferometer as shown in Fig. 1. The production position of the X2-mode He-ECWC plasma is discussed in detail in Section 3.4.

3.3. Hydrogen removal by He-ECWC

Fig. 6 shows the number of retained H_2 molecules during the H_2 tokamak discharges and the subsequent

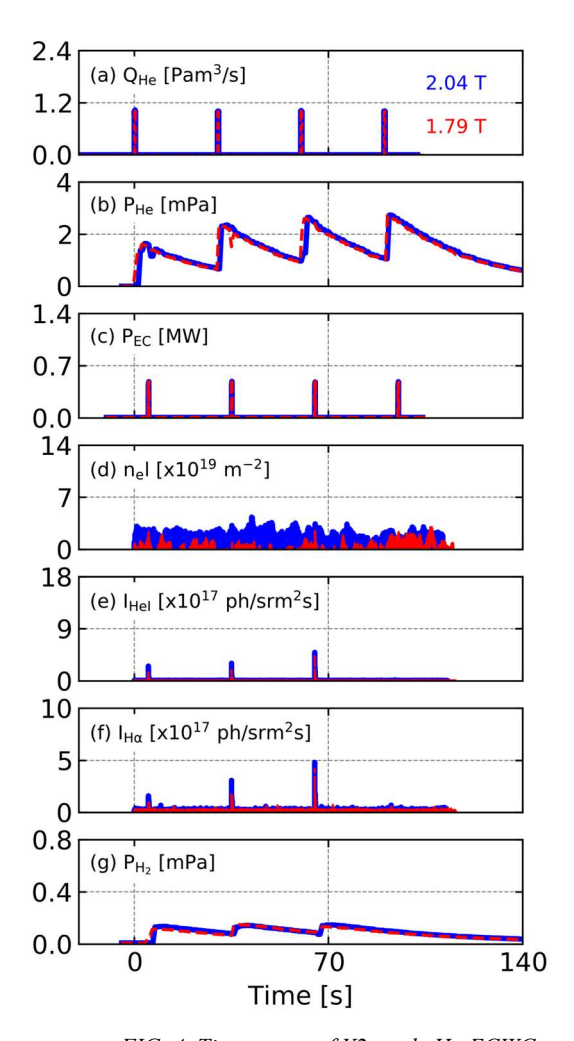


FIG. 4. Time traces of X2-mode He-ECWC sequences at $f_{EC} = 110$ GHz for $B_T = 1.79$ (Shot No. of E101168) and 2.04 T (E101166). Meanings of the lines are the same as Fig. 2.

He-ECWC experiment. The number of retained H_2 molecules by the 4 shots of the H_2 tokamak discharge was 3.1 \times 10²¹. The number of removed H_2 molecules by the 4 sequences (or 16 pulses) of the He-ECWC was 0.5 \times 10²¹, corresponding to 16% of the retained H_2 molecules.

Table 1 summarizes the number of removed H_2 molecules per He-ECWC pulse and the ratio of the removed H_2 molecules to the residual H_2 molecules. On the O1-mode He-ECWC with $f_{EC} = 82$ GHz, the ratio of the removed H_2 molecules was higher for the pulse with the TPC with n = 0.7 at $B_T = 1.79$ T (Fig. 3 (a2)) and 2.04 T (Fig. 3 (a3)). Comparable H_2 removal ratios were observed for the pulses with the horizontal magnetic configuration at $B_T = 1.79$ T. On the X2-mode He-ECWC with $f_{EC} = 110$ GHz, the ratio of removed H_2 molecules was comparable across all pulses.

On the O1-mode He-ECWC, the plasma shape and the interaction region with the inboard first wall can be controlled by the poloidal magnetic configuration, as shown in Fig. 3. This should result in the different H_2 removal efficiency as shown in Table 1. The interaction region of the O1-mode He-ECWC plasma with the inboard first wall in the TPC with n = 0.7 at $B_T = 1.79$ and 2.04 T is similar to that of the startup plasma. This similarity may explain the higher H_2 removal ratio. For the horizontal magnetic configuration under $B_T = 1.79$ T, the comparable H_2 removal ratio could be attributed to the resonance layer being located near the inboard first wall, as shown in Fig. 1, and the expansion of the He-ECWC plasma throughout the entire volume in the torus, as shown in Fig. 3(d2).

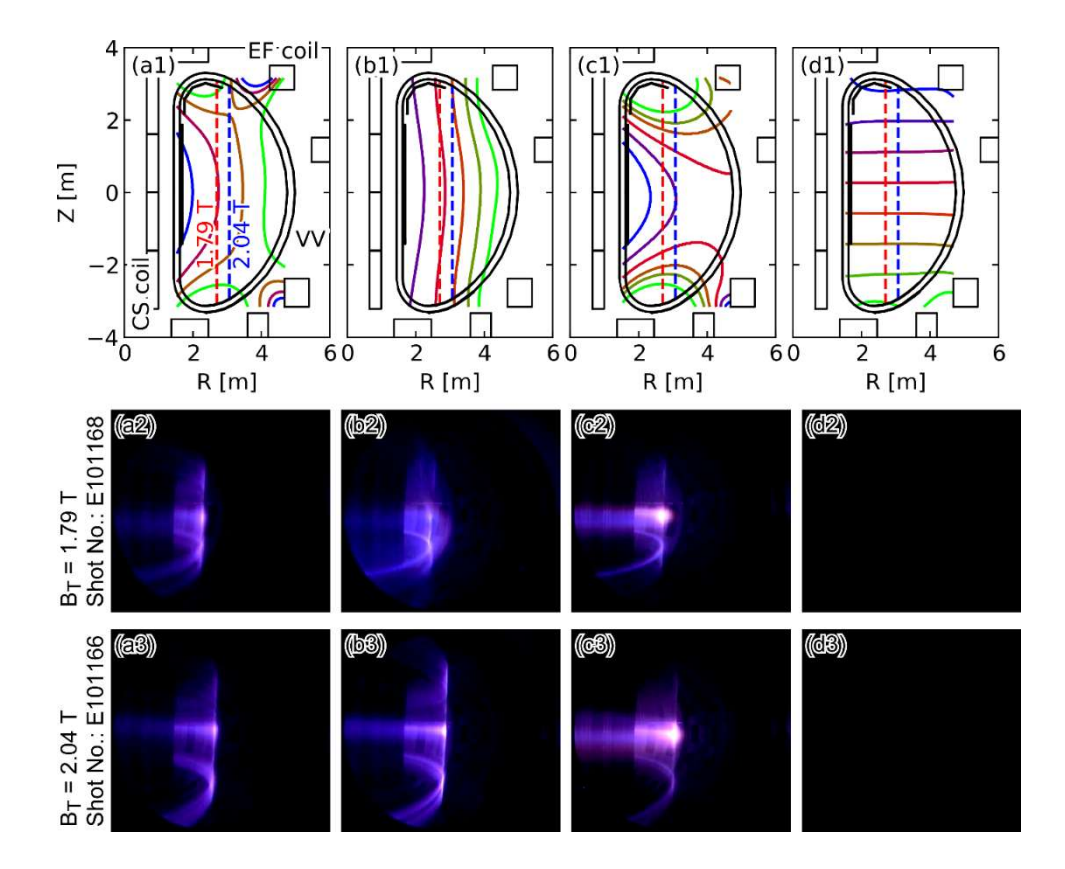


FIG. 5. Poloidal magnetic configurations for X2-mode He-ECWC experiments at $f_{EC} = 110$ GHz for $B_T = 1.79$ and 2.04 T across four pulses, and produced He-ECWC plasmas captured by the visible camera. Meanings of the first-row panel are the same as in Fig. 3 except for panel (b1), which corresponds to the second pulse with TPC with n > 0. The red broken lines show the second harmonic resonance layer for $B_T = 1.79$ T, and the blue ones for $B_T = 2.04$ T. The produced He-ECWC plasmas are captured by the visible camera at (a2–d2) $B_T = 1.79$ T and (a3–d3) 2.04 T.

On the X2-mode He-ECWC, on the other hand, the plasma shape and its interaction region with the inboard first wall cannot be controlled by the poloidal magnetic configuration, as shown in Fig. 5. This should result in the comparable $\rm H_2$ removal ratio as observed between all pulses, as shown in Table 1.

3.4. Plasma production position by 110 GHz second harmonic extraordinary mode EC wave

To investigate the production positions of the X2-mode He-ECWC plasma with $f_{EC} = 110$ GHz at $B_T = 1.79$ and 2.04 T, the He-ECWC plasma is reconstructed using CAD and compared with the image captured by the visible camera, as shown in Fig. 7. In both B_T cases, the radial and height positions of the plasma reconstructed at the inter-section point of the first-pass EC ray and the

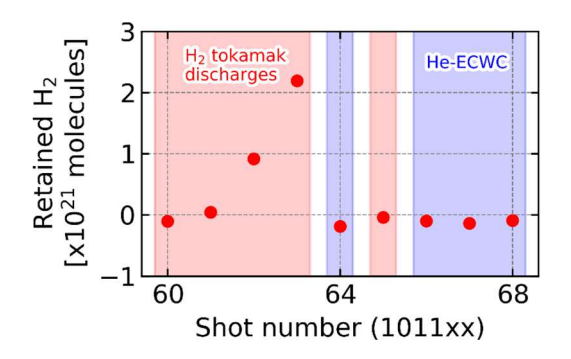


Fig. 6. The number of retained H₂ molecules per shot during the H₂ tokamak discharges and the subsequent He-ECWC experiment.

resonance layer are almost consistent with those of the observed plasma. Although the height position of the plasma reconstructed at the intersection point of the second pass (reflected) EC ray and the resonance layer is inconsistent with the observed plasma in both B_T cases, the downside plasma could be produced at the intersection point of the second pass EC ray and the resonance layer. This is because the plasma position rises when the resonance layer moves closer to the inboard first wall as B_T decreases as shown in Fig. 7 (a) and (c).

3.5. Evaluation of single-pass EC absorption rate

[Right hand page running head is the paper number in Times New Roman 8 point bold capitals, centred]

Table 1. The number of removed H_2 molecules per He-ECWC pulse evaluated by the time integral of the P_{H2} time trace, as shown in Figs. 2 (g) and 4 (g), from the initiation of the EC pulse to that of the next pulse (30 s). The value inside the bracket indicates the ratio of the number of removed H2 molecules to that of residual H2 molecules.

Shot No.	f _{EC} [GHz]	$B_{\mathrm{T}}\left[\mathrm{T}\right]$	The number of removed H ₂ molecules [x10 ¹⁹ molecules]			
			1st pulse	2nd	3rd	4th
E101167	82	1.79	2.3 (0.9%)	1.7 (0.7%)	1.6 (0.6%)	2.4 (0.9%)
E101164		2.04	3.1 (1.0%)	2.3 (0.7%)	2.1 (0.7%)	1.9 (0.6%)
E101168	110	1.79	0.9 (0.4%)	1.2 (0.5%)	1.1 (0.5%)	-
E101166		2.04	1.0 (0.4%)	1.2 (0.5%)	1.2 (0.5%)	-

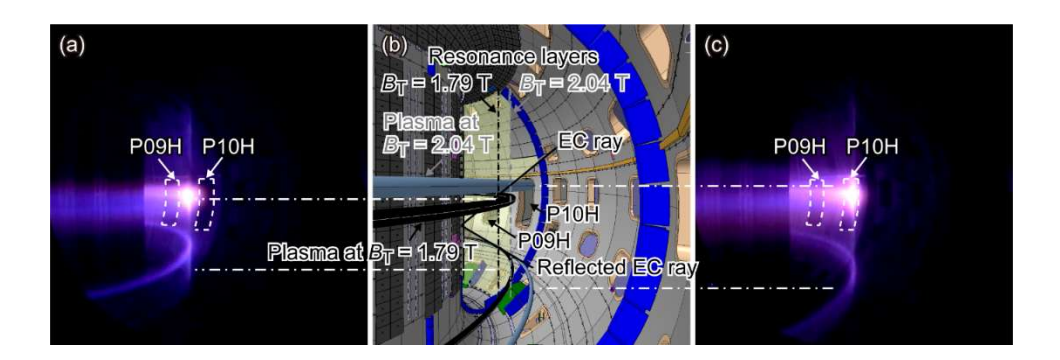


FIG. 7. Production positions of the X2-mode He-ECWC plasma at the third pulse with $f_{EC} = 110$ GHz at $B_T =$ 1.79 and 2.04T. (a) He-ECWC plasma at $B_T = 1.79$ T captured by the visible camera, (b) He-ECWC plasma at $B_T = 1.79$ T captured by the visible camera, (b) He-ECWC plasma at $B_T = 1.79$ T captured by the visible camera, (b) He-ECWC plasma at $B_T = 1.79$ T captured by the visible camera, (b) He-ECWC plasma at $B_T = 1.79$ T captured by the visible camera, (c) He-ECWC plasma at $B_T = 1.79$ T captured by the visible camera, (b) He-ECWC plasma at $B_T = 1.79$ T captured by the visible camera, (c) He-ECWC plasma at $B_T = 1.79$ T captured by the visible camera, (b) He-ECWC plasma at $B_T = 1.79$ T captured by the visible camera, (c) He-ECWC plasma at $B_T = 1.79$ T captured by the visible camera, (c) He-ECWC plasma at $B_T = 1.79$ T captured by the visible camera, (d) He-ECWC plasma at $B_T = 1.79$ T captured by the visible camera, (e) He-ECWC plasma at $B_T = 1.79$ T captured by the visible camera, (e) He-ECWC plasma at $B_T = 1.79$ T captured by the visible camera, (e) He-ECWC plasma at $B_T = 1.79$ T captured by the visible camera, (e) He-ECWC plasma at $B_T = 1.79$ T captured by the visible camera, (e) He-ECWC plasma at $B_T = 1.79$ T captured by the visible camera, (e) He-ECWC plasma at $B_T = 1.79$ T captured by the visible camera, (e) He-ECWC plasma at $B_T = 1.79$ T captured by the visible camera, (e) He-ECWC plasma at $B_T = 1.79$ T captured by the visible camera, (e) He-ECWC plasma at $B_T = 1.79$ T captured by the visible camera, (e) He-ECWC plasma at $B_T = 1.79$ T captured by the visible camera, (e) He-ECWC plasma at $B_T = 1.79$ T captured by the visible camera, (e) He-ECWC plasma at $B_T = 1.79$ T captured by the visible camera, (e) He-ECWC plasma at $B_T = 1.79$ T captured by the visible camera, (e) He-ECWC plasma at $B_T = 1.79$ T captured by the visible camera, (e) He-ECWC plasma at $B_T = 1.79$ T captured by the visible camera, (e) He-ECWC plasma at $B_T = 1.79$ T captured by the visible camera, (e) He-ECWC plasma at $B_T = 1.79$ T captured by the visible camera, (e) He-ECWC plasma at $B_T =$ 1.79 or 2.04 T reconstructed by CAD and (c) He-ECWC plasma at $B_T = 2.04$ T captured by the visible camera. In panel (b), the He-ECWC plasma is reconstructed under the assumption that the plasma is produced at the intersection point of the EC ray and the resonance layer.

The first-pass absorption rate of the O1-mode and X2-mode EC waves by the He-ECWC plasma is evaluated based on the temperature increase of carbon tiles facing the EC launcher, as shown in Fig. 8(a). As shown in Fig. 8 (b) and (c), the temperature increase during the He-ECWC is consistent with that observed during EC wave injection without plasma within the experimental variation ($\pm 20\%$). This indicates that most of the injected EC power is not absorbed by the He-ECWC plasma during the first pass for both O1-mode and X2-mode EC waves.

The angular dependence of single-pass absorption rate for the O-mode and X-mode EC waves is calculated [2]. The absorption rate is evaluated by

$$P/P_0 = 1 - e^{-\tau}. (1)$$

Here, P denotes the absorbed power, P_0 the injected power, and τ the optical thickness. The optical thicknesses for O1-mode and X1-mode waves are evaluated as follows:

$$\tau_{1}^{(O)} = \pi^{2} N_{O}^{'} \left(\frac{\omega_{p}}{\omega_{c}}\right)^{2} \left(\frac{v_{t}}{c}\right)^{2} \frac{\left(1 + 2\cos^{2}\theta\right)^{2} \sin^{4}\theta}{(1 + \cos^{2}\theta)^{3}} \frac{L_{B}}{\lambda_{0}}$$
(2)

$$\tau_1^{(X)} = \pi^2 \left(\frac{\omega_p}{\omega_c}\right)^2 (1 + \cos^2 \theta) \frac{L_B}{\lambda_0} \tag{3}$$

Here, ω_p is the electron plasma frequency, ω_c the electron cyclotron frequency, v_t the thermal velocity of the electrons, c the speed of light, θ the injection angle with respect to direction of toroidal magnetic field, and λ_0 the wavelength in vacuum. The refractive index of the O-mode EC wave, $\,N_{O}\,$, can be written in the form

$$N_{O}^{'} = \left\{ \frac{1}{\sin^{2}\theta} \left(1 - \left(\frac{\omega_{p}}{\omega_{c}} \right)^{2} + \frac{1}{2}\sin^{2}\theta - \frac{1}{2}\sqrt{\sin^{4}\theta + 4\left(1 - \left(\frac{\omega_{p}}{\omega_{c}} \right)^{2} \right)^{2}\cos^{2}\theta} \right) \right\}^{\frac{1}{2}}.$$
 (4)

The magnetic field gradient scale length, L_B , can be expressed using the major radius at the resonance layer, R, and the poloidal injection angle, ϕ , measured with respect to the torus axis, as follows:

$$L_B = \left(\frac{1}{R}\cos\theta\sin\phi\right)^{-1}.\tag{5}$$

For the O2-mode and X2-mode EC waves, optical thicknesses are calculated using the following equation:

$$\tau_2^{(O,X)} = 2\pi^2 \left(\frac{\omega_p}{\omega_c}\right)^2 \left(\frac{v_t}{c}\right)^2 \sin^2\theta \left(1 + \cos^2\theta\right) \mu_2^{(O,X)} \frac{L_B}{\lambda_0}.$$
 (6)

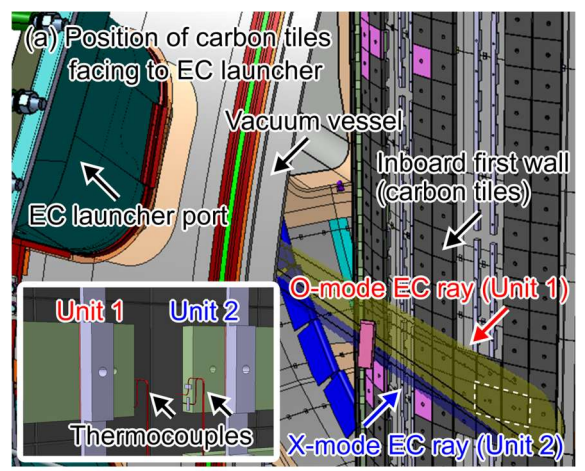
The function $\mu_2^{(O,X)}$ can be written in the form

$$\mu_2^{(O,X)} = \frac{1}{2} \mp \frac{\frac{\sin^4 \theta}{8} + \cos^2 \theta}{\left(\frac{\sin^4 \theta}{16} + \cos^2 \theta\right)^{\frac{1}{2}} (1 + \cos^2 \theta)}.$$
 (7)

The minus (plus) sign on the right-hand side corresponds to the ordinary (extraordinary) mode. The electron density and temperature of the He-ECWC plasma are evaluated from the intensity ratio of He I emission lines [3]: $n_{\rm e} \sim 2 \times 10^{18}$ m⁻³ and $T_{\rm e} < 100$ eV for the O1-mode case and $n_{\rm e} \sim 10^{19}$ m⁻³ and $T_{\rm e} < 16$ eV for the X2-mode case. As shown in Fig. 9, the calculated single pass absorption rates for the O1-mode and X2-mode EC waves at an injection angle of 90° are 10-30%, consistent with the experimental results shown in Fig. 7. The absorption rate of the X1-mode EC wave is found to be 100% across all injection angles. In contrast, the absorption rate of the O2-mode EC wave is less than 1% for all injection angles.

3.6. Possible processes of plasma production

The single-pass absorption rate of the O1-mode is comparable to that of the X2-mode at an injection angle of 90°. Since the plasma produced by the injection of the X2-mode EC wave does not expand along the poloidal magnetic field lines, the initial absorption during the first pass is unlikely to significantly influence plasma expansion. In contrast, the X1-mode EC wave, which has the highest absorption rate, may be more effective in plasma expansion. The injected O1-mode EC wave passes through the resonance layer and reaches the inner first wall. The EC wave reflects at the inner first wall and a portion of the EC wave may convert to X1-mode. The X1-mode EC wave passes through the resonance layer from the high field side, and the power is fully absorbed. This mode conversion process can repeat through reflections between the inboard and outboard first walls, leading to plasma production at the fundamental resonance layer with the different height position via absorption of the X1-mode EC wave power. Because the initial plasma is produced along the fundamental resonance layer, the plasma can expand along the poloidal magnetic field lines. In the



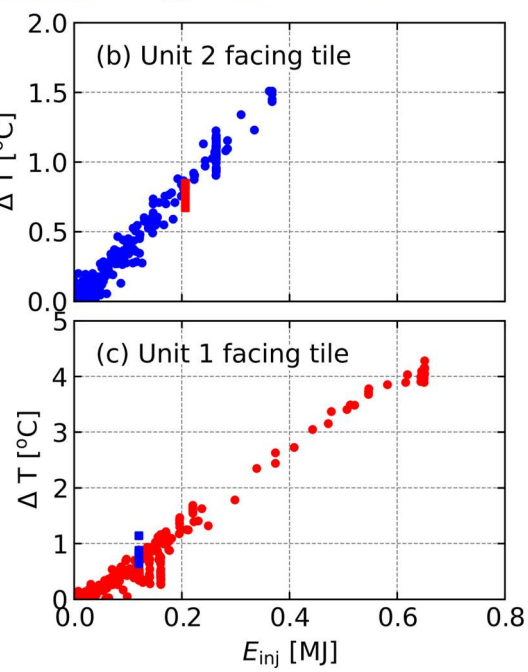


FIG. 8. (a) Position of thermocouple-embedded carbon tiles facing the EC launchers. Temperature increase of the tiles during injection of (b) 82 GHz Omode EC wave (Unit 2) and (c) 110 GHz X-mode EC wave (Unit 1). Closed circles represent EC wave injection without plasma, while closed squares represent injection during He-ECWC.

case of the second harmonic resonance, however, the absorption rates of both X2-mode and O2-mode EC waves are significantly lower than that of the X1-mode EC wave. As a result, the initial plasma is likely produced locally at the intersection of the second harmonic resonance layer and the paths of injected and reflected EC rays.

4. CONCLUSION

Four sequences of He-ECWC following the H₂ tokamak discharges removed 16% of the H₂ molecules retained by the H₂ tokamak discharge. During the O1mode He-ECWC with $f_{\rm EC}$ = 82 GHz, the He-ECWC plasma was expanded along the poloidal magnetic field line. The H₂ removal ratio relative to the residual H₂ molecules per pulse was higher for the pulse with the TPC at n = 0.7 under $B_T = 1.79$ and 2.04 T. This could be because the He-ECWC plasma was produced on the inboard first wall where the start-up phase of the H₂ tokamak plasma was produced. A comparable H₂ removal ratio was observed for the pulse with the horizontal magnetic configuration at $B_T = 1.79$ T. One reason was expected to be the resonance layer was formed near the inboard first wall and the He-ECWC plasma expanded throughout the entire volume in the torus. In contrast, the X2-mode He-ECWC plasma was

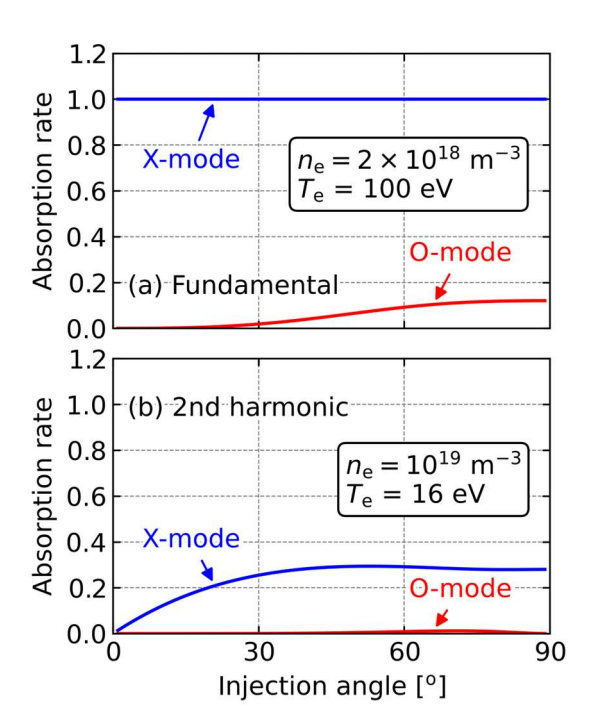


FIG. 9. Angular dependence of the single-pass absorption rate for (a) fundamental and (b) second harmonic O-mode and X-mode EC waves. The electron density and temperature used in the calculations are shown in the insert.

produced locally at the intersection point of the EC ray and the resonance layer within the second pass of the EC ray. The temperature increase in the carbon tiles facing the EC launchers indicated that the first-pass absorption rates of the O1-mode and X2-mode EC waves were comparable within the experimental variation ($\pm 20\%$). This observation was supported by numerical calculations. The absorption rate of the X1-mode EC wave was evaluated to be 100% across all injection angles. Mode conversion from the O1-mode to the X1-mode during reflection at the wall may play an important role in plasma expansion. The initial plasma may be produced along the fundamental resonance layer by the X1-mode EC wave converted from the O1-mode through multiple reflection at the wall. This plasma may then expand along the poloidal magnetic field lines. For the X2-mode injection, on the other hand, because the absorption rate of the O2-mode converted from the X2-mode was lower than that of the X2-mode, the plasma could be produced locally at the intersection of first and second passes of the EC ray and the resonance layer. The localized plasma production could be one of the reasons why the X2-mode He-ECWC plasma did not expand along the poloidal magnetic field lines.

REFERENCES

- [1] FUKUMOTO, M. NAKANO, T., ITAMI, K., ISAYAMA, A., SUZUKI, T., KUBO, H., Nucl. Mater. Energy **12** (2017) 725–732.
- [2] BORNATICI, M., CANO, R., BARBIERI, De O., ENGELMANN, F., Nucle. Fusion 23 9 (1983) 1153-1257.
- [3] NAKANO, T., KUBO, H., ASAKURA N., J. Phys. B: At. Mol. Opt. Phys. 43 (2010) 144014.